

**RATIONAL CATALYST DESIGN FOR THE REMOVAL OF ORGANIC
CONTAMINANTS FROM WATER**

CHAITRA SHANTHARAM SHENOY



**DEPARTMENT OF CHEMICAL ENGINEERING
INDIAN INSTITUTE OF TECHNOLOGY DELHI**

JUNE 2025

© Indian Institute of Technology Delhi (IITD), New Delhi, 2025

**RATIONAL CATALYST DESIGN FOR THE REMOVAL OF ORGANIC
CONTAMINANTS FROM WATER**

by

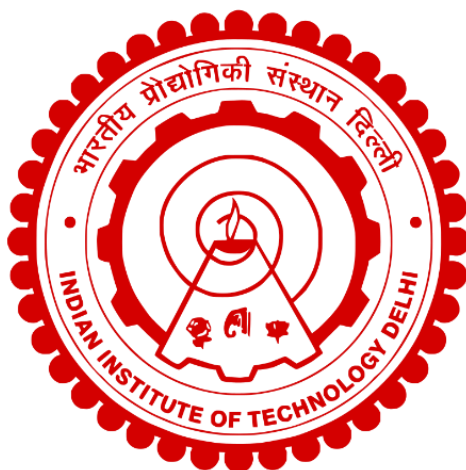
Chaitra Shantharam Shenoy

Department of Chemical Engineering

Submitted

in fulfilment of the requirements of the degree of Doctor of Philosophy

to the



Indian Institute of Technology Delhi

June 2025

*Dedicated to my grandparents (ajja and mamama),
parents and Ajay*

Certificate

This is to certify that the dissertation entitled “**Rational Catalyst Design for the Removal of Organic Contaminants from Water**” being submitted by **Chaitra Shantharam Shenoy** to the Indian Institute of Technology Delhi, for fulfilment of the requirements for the award of **Doctor of Philosophy** in Chemical Engineering is a record of bona-fide research work carried out by her. She has worked under my supervision and has fulfilled the requirements, which to my knowledge, has reached the requisite standard for the submission of the thesis. The results presented in this thesis have not been submitted, in part or full, to any other university or institute for the award of any degree or diploma.

Prof. M. Ali Haider

Professor

Department of Chemical Engineering

Indian Institute of Technology Delhi

Hauz Khas, New Delhi - 110016

Acknowledgments

It is said that what is written for you in your destiny cannot be averted. I am a strong believer in that statement. Also, I firmly hold that no journey can find its true destination without the guiding hand and blessings of the Almighty. I humbly bow down in reverence and gratefulness to the Almighty God, who showed me the light even when my eyes could not see what lay ahead. It is only due to His ample boons and mercy that I have been able to embark on this journey and complete it with resilience, perseverance and clarity. Among His countless blessings, I am extremely grateful for my parents, Shantharam Shenoy and Asha Shenoy, my first teachers in the school of life. They instilled virtues and principles early on, moulding me into a better human. Without their unwavering support, motivation, sacrifice, care, love and prayers, I most definitely would not be standing here today.

My journey at IIT Delhi has been made possible by the many individuals I have had the privilege of crossing paths with during my Ph.D., each contributing to an enriching experience. To begin with, I would like to express sincere gratitude to my advisor, Prof. M. Ali Haider, who gave me an opportunity to pursue a Ph.D. under his guidance. I found his intellect, dedication and expertise in solving problems quite inspiring. The meticulously designed courses are something that I have thoroughly enjoyed, challenging me to think and further highlighting his love for science. Prof. Shelaka Gupta from IIT Hyderabad, also my senior from the REC Lab, played no less a role than an advisor in guiding me through my Ph.D. journey. Her support and guidance were instrumental in helping me navigate challenges, while our regular discussions greatly enhanced my ability to conduct research more effectively.

I would also like to thank my committee members – Prof. Divesh Bhatia, Prof. Manjesh Kumar and Prof. K. A. Subramanian for their insightful analyses and fitting questions that greatly improved the quality of the research. I wish to extend my thanks to Dr. Tuhin Suvra Khan,

CSIR-IIP Dehradun and Dr. Uzma Anjum for assisting me in solving and investigating the theoretical work. Dr. Imteyaz Alam and Dr. Ruchi Jain provided invaluable guidance in setting up experiments and played a crucial role in helping me grasp the fundamentals of reactor operation and catalyst synthesis. Their strong work ethic served as a constant source of inspiration, and the insightful discussions I had with them greatly enriched my understanding — for this, I am truly grateful.

My life at IIT Delhi would be incomplete (and far less fun) without the REC Lab members – Dr. Haseena, Dr. Fatima, Ashutosh, Deepak, Jayendran, Ussama, Iqra, Jyotsana, Adarsh, Mukesh, Mahdiyar and Sharad, whose presence turned challenges into manageable moments and have stood by me through the highs and lows, making this journey all the more memorable. It has been a privilege to mentor dual degree students Kirti Verma and Athira Ajithkumar. Through this experience, they helped me understand, at a fundamental level, the responsibilities and nuances of effective mentorship and for this, I am deeply grateful.

It is not just the individuals I came across at IIT Delhi that have influenced my life and Ph.D. journey, but also my friends who are nothing short of family. I am greatly indebted to Dr. Sagar Bharathraj (Sagar Anna as I fondly call him), who, like his name, has offered me infinite belief, positivity, encouragement and patience. I have always considered his presence a godsend that I had never even prayed for, but I was blessed with, and for that, I am eternally grateful. Prasad and Prathvi, who have been a source of entertainment and support ever since I met them at NITK Surathkal. They taught me to enjoy life and gradually helped me overcome my introversion. I have known the true meaning of friendship because of Anand Gaikaiwari. He has been a whetstone to my wit, and his company is something I have and will always cherish. A heartfelt thanks to my school friend, Bhagyashree Nair, who has been through life's ups and downs with me, constantly sharing words of encouragement and being a source of strength.

This note of thanks would remain lacking without expressing my gratitude to my family. I am especially thankful to my ajja (Late. Shri Leeladhar Nayak) and mamama (Sudha Leeladhar Nayak). Even though they did not understand my work, have always supported, loved and cared for me. My ajja especially motivated me to try again and again constantly, and never to give up. My mamama, being the kindest and most gentle soul I have ever come across, has always imparted patience, wisdom and faith when things did not go according to the plan. They have, without doubt, shaped me to be the person I am today, and I feel lucky to have grown up with such grandparents. My sister, Prithvi Shenoy, has always had my back through all the seasons of life. Through her presence, I learned to stay resilient in difficult times. I am profoundly grateful to her for always being my pillar of strength, my greatest inspiration and my source of joy.

I would also like to extend my thanks to my parents-in-law, Suresh Kini and Surekha Kini. With their constant encouragement, care, and belief in me, the path felt lighter and more manageable than I could have anticipated. I am grateful to my brother-in-law, Kiran Kini, whose warmth and generosity made my trip to the United States for a conference not only possible but also comfortable. His kindness gave me a home away from home, without which this experience would not have been the same. Last but certainly not least, I feel truly fortunate to have found a compassionate and understanding partner in Ajay Kini. Despite our different educational backgrounds, he has embraced my journey with patience, grace, and unwavering support. Through every high and low, his presence has brought joy, resilience, and a sense of calm. His quiet encouragement has not only helped me navigate challenges but also discover my inner strength. This Ph.D. journey has been all the more fulfilling because of him, and for that, I am profoundly grateful.

Chaitra Shantharam Shenoy

Abstract

The organic contaminants released from various industries, due to their carcinogenic nature and inability to degrade naturally, pose a serious threat to human health and the environment. Of the existing treatment techniques for the removal of these organic pollutants from water, catalytic treatment is a viable practice as it is economically feasible, leads to complete mineralization of the pollutants and can be conducted at moderate reaction conditions. This transformation of organic contaminants is aided by transition metals and thus, it is deemed essential to rationally design the catalysts. In this direction, catalytic reactions (hydrodechlorination (HDC) reaction and oxidation reaction) of various contaminants (trichloroethylene (TCE), 4-chlorophenol (4-CP) and ethylene glycol (EG)) using density functional theory (DFT) simulations combined with microkinetic modeling (MKM) are undertaken. A few experiments are also carried out involving TCE as a model impurity.

In the present work, an attempt is made to gain mechanistic insights on the reactivity of the Pd catalyst, which is the most widely employed catalyst for HDC reactions. Towards this, the HDC reaction of TCE, incorporating DFT calculations, is simulated over different facets (terrace Pd (111) and Pd (100), undercoordinated Pd (211) and Pd (110)) of a Pd catalyst. TCE undergoes dechlorination to form a hydrocarbon intermediate followed by hydrogenation to form ethene or ethane. On the Pd catalyst, TCE binds with a high binding energy (B.E.) of -178 kJ/mol over the Pd (110) surface. The chlorine atoms released as a result of dechlorination tend to block the active sites, thereby poisoning the surface with high binding energies (B.E. > -160 kJ/mol) on all the surfaces. The removal of surface chlorine is facilitated by its reaction with surface hydrogen to form hydrogen chloride. The terrace sites display comparatively lower activation energies for the formation of hydrogen chloride in contrast to the undercoordinated sites, which suggests the ease of removal of Cl as HCl from the terrace sites. The structure sensitivity in the TCE HDC reaction could possibly arise due to the differences in the energetics of Cl removal on different Pd facets.

In addition, to understand the role of the support in the HDC reaction of TCE, few experiments are also conducted by employing Pd metal supported over carbon (Pd/C) and titania (Pd/TiO_{2(C)} and Pd/TiO_{2(S)}, wherein the subscripts (C) and (S) stand for commercial and synthesized TiO₂, respectively). TCE HDC follows first order reaction kinetics. In this study, it is observed that on increasing the temperature, the conversion increases over the three catalysts. However, the conversion increases drastically over the TiO₂-supported Pd catalyst compared to the Pd/C catalyst. The variation in the concentration with temperature is utilized to calculate the apparent

activation energies (E_{app}). Herein, the E_{app} over the Pd/C catalyst is calculated to be 21.2 kJ/mol, which is higher than that calculated over the Pd/TiO_{2(C)} catalyst (E_{app} = 13.6 kJ/mol) and Pd/TiO_{2(S)} catalyst (E_{app} = 12.4 kJ/mol). Furthermore, the DFT studies reveal lower adsorption energy of chlorine over Pd₄/TiO₂ compared to the Pd (111) slab, highlighting the role of the titania support.

Addition of a second metal to the parent metal (Pd) has proved to be beneficial as it leads to improved stability, activity and selectivity towards the desired product compared to the parent metal. Herein, a combined DFT and MKM study for the HDC of 4-CP is performed over the terrace (111) sites of the Pd metal and A₃B type alloys with coinage metals (A-Pd, B-Cu, Ag and Au). 4-CP undergoes dechlorination followed by hydrogenation to form phenol. The Pd₃Ag surface displays the lowest barrier (44 kJ/mol) for the C-Cl bond dissociation step compared to the monometallic Pd surface (71 kJ/mol). The trend in the reactivity follows: Pd₃Ag > Pd₃Au > Pd > Pd₃Cu. The high turnover frequency (TOF) over the Pd₃Ag surface could be attributed to the ease of C-Cl bond dissociation, whereas the low TOF over the Pd₃Cu surface can be due to the high binding energy of 4-CP molecule. For the C-Cl bond dissociation step, a positive degree of rate control is observed, which suggests that the step is crucial in ascertaining the HDC rate.

Further, to understand the effect of the catalyst particle size on the oxidation reaction of EG, different transition metals and nanoclusters are screened by building a MKM. EG oxidizes to form glycolic acid and oxalic acid. Two different routes are explored for this oxidation reaction – direct metal-assisted oxidation route and the O and OH-assisted oxidation route. The transition metals display considerably higher TOF via the O and OH-assisted route compared to the metal-assisted route (TOF is 4 to 5 orders of magnitude lower). A high selectivity towards glycolic acid is reported over all the nanoclusters and transition metals via the O and OH-assisted route compared to oxalic acid formation. In addition, on moving from metal surfaces to nanoclusters, that is, reducing the size of the catalyst, the Au₁₃ nanocluster is observed to lie at the top of the volcano plot with a high selectivity towards glycolic acid.

In all, this dissertation presents a brief outline on developing catalytic materials for the removal of organic contaminants in water, accomplished by employing theoretical tools, that can aid in the rational design of catalysts by providing mechanistic insights and trends in the activity and selectivity of the catalysts.

सार

विभिन्न उद्योगों से निकलने वाले कार्बनिक प्रदूषक, जो कैसरजन्य प्रकृति के होते हैं और स्वाभाविक रूप से नष्ट नहीं हो सकते, मानव स्वास्थ्य और पर्यावरण के लिए गंभीर खतरा पैदा करते हैं। जल से इन कार्बनिक प्रदूषकों को हटाने के लिए उपलब्ध उपचार तकनीकों में, उत्प्रेरक उपचार एक व्यावहारिक विकल्प है क्योंकि यह आर्थिक रूप से किफायती है, प्रदूषकों का पूर्ण खनिजीकरण करता है और इसे मध्यम प्रतिक्रियात्मक परिस्थितियों में किया जा सकता है। इन कार्बनिक प्रदूषकों के रूपांतरण में संक्रमण धातुएँ सहायक होती हैं, और इसलिए उत्प्रेरकों की तार्किक रूप से डिज़ाइनिंग आवश्यक मानी जाती है।

इस दिशा में, कार्बनिक प्रदूषकों (ट्राइक्लोरोएथिलीन (TCE), 4-क्लोरोफेनोल (4-CP) और एथिलीन ग्लाइकोल (EG)) की हाइड्रोडिक्लोरीनेशन (HDC) और ऑक्सीकरण प्रतिक्रियाओं का अध्ययन डेंसिटी फंक्शनल थ्योरी (DFT) सिमुलेशन और माइक्रोकाइनेटिक मॉडलिंग (MKM) के संयोजन से किया गया है। कुछ प्रयोगात्मक अध्ययन भी किए गए हैं, जिनमें TCE को एक मॉडल अशुद्धि के रूप में लिया गया है।

इस कार्य में, Pd उत्प्रेरक की प्रतिक्रियाशीलता पर यांत्रिक अंतर्दृष्टि प्राप्त करने का प्रयास किया गया है, जो HDC प्रतिक्रियाओं के लिए सबसे व्यापक रूप से प्रयुक्त उत्प्रेरक है। इसके लिए, TCE की HDC प्रतिक्रिया को विभिन्न Pd सतहों (टैरेस Pd (111) और Pd (100), अंडरकोऑर्डिनेटेड Pd (211) और Pd (110)) पर DFT गणनाओं को शामिल करते हुए सिमुलेट किया गया है। TCE डी-क्लोरीनेशन के बाद हाइड्रोजन के साथ अभिक्रिया करता है और इथीन या इथेन बनाता है। Pd उत्प्रेरक पर TCE Pd (110) सतह पर -178 kJ/mol की उच्च बाइंडिंग ऊर्जा के साथ बंधता है। डी-क्लोरीनेशन के फलस्वरूप मुक्त हुए क्लोरीन परमाणु सक्रिय स्थलों को अवरुद्ध करते हैं, जिससे सतह जहर का शिकार होती है, क्योंकि इनकी बाइंडिंग ऊर्जा सभी सतहों पर अधिक होती है (B.E. $> -160 \text{ kJ/mol}$)। सतह पर हाइड्रोजन के साथ क्लोरीन की प्रतिक्रिया से हाइड्रोजन क्लोराइड बनती है, जिससे क्लोरीन हटाना संभव होता है। टैरेस साइट्स पर HCl बनने की सक्रियण ऊर्जा अंडरकोऑर्डिनेटेड साइट्स की तुलना में कम पाई गई, जिससे टैरेस साइट्स पर Cl को HCl के रूप में हटाना अधिक आसान प्रतीत होता है। इससे यह स्पष्ट होता है कि TCE HDC प्रतिक्रिया में Pd सतहों की संरचनात्मक संवेदनशीलता Cl को हटाने की ऊर्जा में अंतर के कारण उत्पन्न हो सकती है।

साथ ही, TCE की HDC प्रतिक्रिया में सपोर्ट की भूमिका को समझने के लिए कुछ प्रयोग भी किए गए, जिनमें Pd को कार्बन (Pd/C) और टाइटेनिया (Pd/TiO₂(C) और Pd/TiO₂(S), जहाँ (C) और (S) क्रमशः वाणिज्यिक और संश्लेषित टाइटेनिया को दर्शाते हैं) पर सहारा दिया गया है। TCE HDC प्रथम क्रम की अभिक्रिया गति का पालन करता है। इस अध्ययन में पाया गया कि तापमान बढ़ाने पर तीनों उत्प्रेरकों पर रूपांतरण में वृद्धि होती है, परंतु TiO₂-समर्थित Pd उत्प्रेरकों पर यह वृद्धि Pd/C की तुलना में कहीं अधिक होती है। तापमान के साथ सांद्रता में अंतर का उपयोग कर के प्रकट सक्रियण ऊर्जा (E_{app}) की गणना की गई है। Pd/C उत्प्रेरक के लिए $E_{app} = 21.2$ kJ/mol, जबकि Pd/TiO₂(C) के लिए $E_{app} = 13.6$ kJ/mol और Pd/TiO₂(S) के लिए $E_{app} = 12.4$ kJ/mol पाया गया। DFT अध्ययन यह भी दिखाते हैं कि Pd₄/TiO₂ पर क्लोरीन का एडसॉर्शन Pd (111) सतह की तुलना में कम होता है, जो टाइटेनिया सपोर्ट की भूमिका को रेखांकित करता है।

मूल धातु (Pd) में एक द्वितीय धातु जोड़ना लाभकारी सिद्ध हुआ है क्योंकि इससे उत्प्रेरक की स्थिरता, सक्रियता और चयनात्मकता बेहतर होती है। इस संदर्भ में, 4-CP की HDC प्रतिक्रिया के लिए Pd (111) टैरेस साइट्स और कॉइनज धातुओं (Pd-Cu, Pd-Ag और Pd-Au) के A₃B प्रकार के मिश्रधातु सतहों पर DFT और MKM का संयुक्त अध्ययन किया गया है। 4-CP डीक्लोरीनेशन के बाद फिनोल में परिवर्तित होता है। Pd₃Ag सतह पर C-Cl बॉन्ड टूटने की ऊर्जा अवरोध सबसे कम (44 kJ/mol) पाया गया, जो मोनोमेटालिक Pd सतह (71 kJ/mol) की तुलना में काफी कम है। प्रतिक्रियात्मकता की प्रवृत्ति इस प्रकार है: Pd₃Ag > Pd₃Au > Pd > Pd₃Cu। Pd₃Ag सतह पर उच्च टर्नओवर फ्रिक्वेंसी (TOF) C-Cl बंध के आसानी से टूटने के कारण है, जबकि Pd₃Cu पर TOF कम है क्योंकि 4-CP अणु की बाइंडिंग ऊर्जा अधिक होती है। C-Cl बंध टूटने के चरण पर प्रतिक्रिया दर नियंत्रण की सकारात्मक डिग्री पाई गई है, जो दर्शाती है कि यह चरण HDC दर निर्धारित करने में निर्णायक है।

इसके अलावा, EG के ऑक्सीकरण प्रतिक्रिया में उत्प्रेरक कण आकार के प्रभाव को समझने हेतु विभिन्न संक्रमण धातुओं और नैनोकणों का MKM मॉडलिंग द्वारा अध्ययन किया गया है। EG का ऑक्सीकरण ग्लायकोलिक अम्ल और ऑक्सालिक अम्ल में होता है। इस ऑक्सीकरण के दो मार्ग अध्ययन किए गए: प्रत्यक्ष धातु-सहायित मार्ग और O एवं OH-सहायित मार्ग। O और OH-सहायित मार्ग पर सभी संक्रमण धातुओं पर TOF धातु-सहायित मार्ग की तुलना में 4-5 गुणा अधिक पाया गया। सभी नैनोकणों और धातुओं पर ग्लायकोलिक अम्ल के लिए उच्च चयनात्मकता देखी गई। जब धातु सतहों से नैनोकणों की ओर बढ़ा गया (अर्थात् उत्प्रेरक आकार घटाया गया), तब पाया गया कि Au₁₃ नैनोकण वोल्केनो प्लॉट के शीर्ष पर स्थित है और ग्लायकोलिक अम्ल के प्रति उच्च चयनात्मकता दर्शाता है।

अंततः, यह शोध कार्य जल में मौजूद कार्बनिक प्रदूषकों को हटाने हेतु उत्प्रेरक पदार्थों के विकास की रूपरेखा प्रस्तुत करता है, जिसे सैद्धांतिक उपकरणों के उपयोग से पूरा किया गया है। यह दृष्टिकोण उत्प्रेरकों की तार्किक डिज़ाइनिंग में सहायक हो सकता है, क्योंकि यह गतिविधि और चयनात्मकता में प्रवृत्तियों और यांत्रिक अंतर्दृष्टियों को उजागर करता है।

Content

Certificate	i
Acknowledgements	ii
Abstract	v
Content	x
List of Figures	xiii
List of Tables	xx
Chapter 1	1
Introduction	1
1.1 Background and Motivation.....	1
1.2 Objectives.....	22
1.3 Thesis Organisation.....	23
1.4 References	26
Chapter 2	35
Rational Catalyst Design for the Removal of Organic Contaminants	35
2.1 Introduction	35
2.2 Effect of particle size.....	37
2.3 Effect of support.....	44
2.4 Catalyst deactivation and regeneration techniques	49
2.5 Alloying Strategies	55
2.6 Effect of Solvent.....	59
2.7 Catalytic Transfer Hydrogenation (CTH)	61
2.8 Computational Studies	64
2.9 Oxidation Reactions	67
2.10 Outlook.....	69
2.11 References	70
Chapter 3	78
Methodology	78
3.1 Computational Methods	78
3.1.1 Density Functional Theory (DFT).....	78
3.1.2 Microkinetic Modelling (MKM)	87
3.1.3 Modelling of catalytic surfaces and sites.....	97

3.2 Experimental Methods	101
3.2.1 Catalytic Reactors.....	101
3.2.2 High-performance liquid chromatography (HPLC) technique.....	103
3.3 References	105
Chapter 4	107
Reactivity of Transition Metal Catalysts for Hydrodechlorination of Trichloroethylene	107
4.1 Introduction	107
4.2 Methodology	110
4.3 Results and Discussion.....	111
4.4 Summary	131
4.5 References	132
Chapter 5	138
Supported Transition Metal Catalysts for Hydrodechlorination of Trichloroethylene.	138
5.1 Introduction	138
5.2 Methodology	141
5.2.1 Experimental Methods.....	141
5.2.1.1 Synthesis of anatase TiO ₂ nanoparticles	141
5.2.1.2 Synthesis of Pd/TiO ₂ (s).....	142
5.2.1.3 Catalytic Activity	142
5.2.2 Computational Methods	143
5.3 Results and Discussion.....	144
5.4 Summary	156
5.5 References	157
Chapter 6	160
Design of Bimetallic Alloys for Hydrodechlorination of 4-Chlorophenol.....	160
6.1 Introduction	160
6.2 Methodology	163
6.3 Results and Discussion.....	167
6.4 Summary	182
6.5 References	183
Chapter 7	189
Reactivity of Transition Metal Nanoclusters for Selective Oxidation of Ethylene Glycol	189

7.1 Introduction	189
7.2 Methodology	193
7.3 Results and Discussion.....	195
7.4 Summary	208
7.5 References	209
Chapter 8	213
Conclusions and Outlook	213
Appendix A	218
Appendix B.....	227
Appendix C.....	232
Appendix D.....	237
Biodata	

List of Figures

Figure 1.1 Origins of water contamination from pollutants discharged by various sectors	1
Figure 1.2 List of organic pollutants released from different industries	2
Figure 1.3 Removal of contaminants from industrial wastewater via the adsorption technique	4
Figure 1.4 A schematic displaying the air stripping technique for pollutant removal	5
Figure 1.5 A schematic for the ozonation method	6
Figure 1.6 A schematic displaying the working of the electro-coagulation technique	7
Figure 1.7 Aerobic biodegradation of pollutants present in industrial wastewater.....	8
Figure 1.8 A representation of the working in a membrane filtration technique	9
Figure 1.9 The varying length scales in heterogeneous catalysis	12
Figure 1.10 The effect of particle size in a cubic close-packed cuboctahedral-shaped Pd nanoparticle.....	13
Figure 1.11 The effect of increasing the chloride concentration on the turnover frequency (TOF) for the bimetallic Pd/Au nanoparticles and monometallic Pd catalysts (Pd NPs and Pd/Al ₂ O ₃). Adapted from Ref ⁷⁵	16
Figure 1.12 Bridging material and pressure gaps through theoretical catalyst design.....	18
Figure 1.13 Catalytic hydrodechlorination and oxidation reactions of the selected model contaminants	21
Figure 2.1 Sabatier principle for optimum binding of the adsorbate	36
Figure 2.2 Coordination numbers of various facets for a cuboctahedra nanoparticle	37
Figure 2.3 The effect of particle size on the fraction of different catalytic sites. Adapted from Ref ⁶	38
Figure 2.4 The formation of the density of states	39
Figure 2.5 The shift in the d-band centres over a)Ru and b)Ag for the adsorption of O atom	41
Figure 2.6 The structure sensitivity of dehydrogenation and hydrogenolysis reaction of cyclohexane over Pt step sites and kink sites. Adapted from Ref ¹⁴	42
Figure 2.7 The HDC reaction of 2,4-dichloro-phenoxyacetic acid (2,4-D) over Pd catalyst. Adapted from Ref ²⁷	45
Figure 2.8 The kinetic studies for the HDC reaction of diclofenac over supported Pd catalyst. Adapted from Ref ³⁸	47

Figure 2.9 Initial turnover frequencies over the Pd nanoparticles and Pd/Al ₂ O ₃ catalyst with respect to (a) chloride poisoning and (b) sulphide poisoning. Reproduced from Ref ⁵⁸	52
Figure 2.10 The regeneration cycles over Rh/C and Ru/C for the HDC of TCM. Reproduced from Ref ⁶⁵	54
Figure 2.11 The unit cell and arrangement of intermetallic alloys in a fcc crystal structure ..	56
Figure 2.12 The geometric and electronic effects on alloying.....	57
Figure 2.13 Turnover frequency for the HDC of 4-chlorophenol over the AgPd _x nanocrystals. Reproduced from Ref ⁷¹	58
Figure 2.14 Formic acid dissociation over Pd catalyst. Reproduced from Ref ⁸⁷	62
Figure 2.15 Binding energies of chlorine over the different facets of Pd. Adapted from Ref ⁹⁵	65
Figure 2.16 Chlorine coverages over transition metal catalysts. Reproduced from Ref ⁹⁸	67
Figure 2.17 The electronic changes observed in Au bulk metal, nanoparticles, clusters and an atom. Reproduced from Ref ¹¹⁵	68
Figure 3.1 Schematic displaying the many-body problem (N-particle system)	80
Figure 3.2 Self-consistent field iterative method to compute the ground state electron density	83
Figure 3.3 Elastic band method tracing the minimum energy path (MEP) for the calculation of the transition state	86
Figure 3.4 The linear relationship displayed in a) Adsorption Energy and b) Transition State Scaling Relationships.....	92
Figure 3.5 Block diagram displaying the structure of microkinetic modeling (MKM) using CatMAP	93
Figure 3.6 A visual representation of the degree of rate control with respect to the intermediate and transition state	95
Figure 3.7 Apparent activation energy (E_{app}) calculated using DRC. Reproduced from Ref ²³	97
Figure 3.8 The slab model consisting of 5 layers for a fcc metal	98
Figure 3.9 Surface relaxation in a fcc metal slab	99
Figure 3.10 The various facets exposed in a fcc crystal on cleaving in a particular direction (Miller indices). Reproduced from Ref ²⁵	100
Figure 3.11 The different binding sites and modes for the adsorption of H atom on fcc metal Cu (100) facet	101
Figure 3.12 Illustrations for the batch and continuous reactors	102

Figure 3.13 Working principle of HPLC.....	104
Figure 4.1 The most stable binding mode of TCE on (a) Pd (111), (b) Pd (211), (c) Pd (100) and (d) Pd (110) surfaces. The Pd atoms are displayed in blue, Cl atoms in green, C atoms in grey and H atom in white color. Distances are marked in Å	113
Figure 4.2 Reactant, transition and product state structures for the first dechlorination step on the Pd (111), Pd (211), Pd (100) and Pd (110) surfaces. The Pd atoms are displayed in blue, Cl atoms in green, C atoms in grey and H atom in white color. Distances are marked in Å	117
Figure 4.3 Reactant, transition and product state structures for the second dechlorination step on the Pd (111), Pd (211) and Pd (100) surfaces. The Pd atoms are displayed in blue, Cl atoms in green, C atoms in grey and H atom in white color. Distances are marked in Å	119
Figure 4.4 Reactant, transition and product state structures for the third dechlorination step on the Pd (111), Pd (211), Pd (100) and Pd (110) surfaces. The Pd atoms are displayed in blue, Cl atoms in green, C atoms in grey and H atom in white color. Distances are marked in Å	122
Figure 4.5 The energy diagram for the dechlorination steps in the HDC reaction of TCE on the Pd (111), Pd (211), Pd (100) and Pd (110) surfaces. Numbers in bold show the intrinsic activation energies of the elementary reaction steps in kJ/mol.....	123
Figure 4.6 The transition state scaling relations obtained for the dechlorination steps of TCE on the Pd (111) (■), Pd (211) (●), Pd (100) (▲) and Pd (110) (◆) surfaces	124
Figure 4.7 The energy diagram for the hydrogenation steps in the HDC reaction of TCE on the Pd (111), Pd (211), Pd (100) and Pd (110) surfaces.....	126
Figure 4.8 The most stable binding modes of chlorine on (a) Pd (111), (b) Pd (211), (c) Pd (100) and (d) Pd (110) surfaces. The Pd atoms are displayed in blue and Cl atoms in green color. Distances are marked in Å	127
Figure 4.9 Reactant, transition and product state structures for the formation of HCl on the Pd (111), Pd (211), Pd (100) and Pd (110) surfaces. The Pd atoms are displayed in blue, Cl atoms in green and H atom in white color. Distances are marked in Å	131
Figure 5.1 The FESEM images and the corresponding EDX mapping of Pd/TiO _{2(C)} (A and B) and Pd/TiO _{2(S)} (C and D) respectively	145
Figure 5.2 The change in the concentration of TCE with respect to time over the a) Pd/C, b) Pd/TiO _{2(C)} and c) Pd/TiO _{2(S)}	147
Figure 5.3 Effect of reaction temperature on the conversion of TCE at 30 mins over the a) Pd/C, b) Pd/TiO _{2(C)} and c) Pd/TiO _{2(S)} catalysts.....	150
Figure 5.4 Arrhenius plots for calculating the apparent activation energies (E_{app}) over the Pd/C, Pd/TiO _{2(C)} and Pd/TiO _{2(S)} catalysts for the HDC reaction of TCE.....	150

Figure 5.5 HR-TEM images for the A) Pd/C, C) Pd/TiO _{2(C)} and E) Pd/TiO _{2(S)} along with their respective calculated particle size distributions (B, D, F)	151
Figure 5.6 XPS studies for the 1) Pd/TiO _{2(C)} and 2) Pd/TiO _{2(S)}	152
Figure 5.7 The binding of chlorine atom on a Pd slab model (a) and Pd ₄ cluster model (b and c). Pd atoms are displayed in blue and Cl atom is displayed in green. Bond lengths are marked in Å.....	153
Figure 5.8 The binding of a chlorine atom in different modes on a Pd ₄ /TiO ₂ model	155
Figure 6.1 The side and top views of the metal surfaces (Pd (111), Pd ₃ Cu (111), Pd ₃ Ag (111) and Pd ₃ Au (111)) employed for the HDC of 4-CP	164
Figure 6.2 The B.E. of 4-CP in the most stable configurations (a(i)-d(i)) and corresponding d-band centers of Pd (111), Pd ₃ Cu (111), Pd ₃ Ag (111) and Pd ₃ Au (111) surfaces (a(ii)-d(ii)). Color code: Pd (dark blue), Cu (orange), Ag (light blue), Au (yellow), C (grey), O (red), H (white), Cl (light green).....	169
Figure 6.3 Initial State (IS), Transition State (TS) and Final State (FS) for the Cl dissociation step on Pd (111), Pd ₃ Cu (111), Pd ₃ Ag (111) and Pd ₃ Au (111) surfaces respectively (a(i)-d(i)). Color Code: Pd (dark blue), Cu (orange), Ag (light blue), Au (yellow), C (grey), O (red), H (white), Cl (light green)	171
Figure 6.4 Binding Energy of 4-CP over the fcc site on the Pd ₃ Au (111) surface.....	173
Figure 6.5 Transition state structures for the hydrogenation step to form phenol without Cl on the surface (I) and with Cl at the fcc site (II) on the Pd (111) surface.....	174
Figure 6.6 Initial State (IS), Transition State (TS) and Final State (FS) for the H addition step to form phenol on Pd (111), Pd ₃ Cu (111), Pd ₃ Ag (111) and Pd ₃ Au (111) surfaces respectively (a(i)-d(i)). Color Code: Pd (dark blue), Cu (orange), Ag (light light blue), Au (yellow), C (grey), O (red), H (white)	175
Figure 6.7 The overall reaction energy diagram for the HDC of 4-CP to form phenol on Pd (111) (-----), Pd ₃ Cu (111) (-----), Pd ₃ Ag (111) (-----) and Pd ₃ Au (111) (-----) surfaces.....	177
Figure 6.8 The turnover frequencies over Pd (111), Pd ₃ Cu (111), Pd ₃ Ag (111) and Pd ₃ Au (111) surfaces in the temperature range 273 K – 873 K.....	178
Figure 6.9 The degree of rate control plots over (i) Pd (111), (ii) Pd ₃ Cu (111), (iii) Pd ₃ Ag (111) and (iv) Pd ₃ Au (111) surfaces with respect to 4-CP B.E., Cl B.E., C ₆ H ₅ OH-Cl* and H-Cl*	179
Figure 6.10 Surface coverage of C ₆ H ₄ OHCl with varying temperatures and pressures over different surfaces ((1) Pd (111), (2) Pd ₃ Cu (111), (3) Pd ₃ Ag (111) and (4) Pd ₃ Au (111)).....	181

Figure 7.1 The production rates for the metal-assisted pathway over different transition metal catalysts for the formation of (a) glycolic acid and (b) oxalic acid, at 473 K and 1 bar (Error bar = 0.2eV)	198
Figure 7.2 The production rates for the metal, O and OH-assisted pathway over different transition metal catalysts for the formation of (a) glycolic acid and (b) oxalic acid, at 473 K and 1 bar (Error bar = 0.2eV)	199
Figure 7.3 The production rates for the metal, O and OH-assisted pathway over the Pt, Au and Ag step, corner, terrace sites and metal clusters for the formation of (a) glycolic acid and (b) oxalic acid, at 473 K and 1 bar (Error bar = 0.2eV)	201
Figure 7.4 The selectivity trends for the metal-assisted pathway over the transition metals for the formation of (a) glycolic acid and (b) oxalic acid, at 473 K and 1 bar (Error bar = 0.2eV)	202
Figure 7.5 The selectivity trends for the metal, O and OH-assisted pathway over the transition metals for the formation of (a) glycolic acid and (b) oxalic acid, at 473 K and 1 bar (Error bar = 0.2eV)	203
Figure 7.6 The selectivity trends for the metal, O and OH-assisted pathway over the Pt, Au and Ag step, corner, terrace sites and metal clusters for the formation of (a) glycolic acid and (b) oxalic acid, at 473 K and 1 bar (Error bar = 0.2eV)	204
Figure 7.7 The trends in the coverage for the metal-assisted pathway over different transition metals for the formation of (a) glycolic acid and (b) oxalic acid, at 473 K and 1 bar (Error bar = 0.2eV)	205
Figure 7.8 The trends in the coverage for the metal, O and OH-assisted pathway over different transition metals for the formation of (a) glycolic acid and (b) oxalic acid, at 473 K and 1 bar (Error bar = 0.2eV)	206
Figure 7.9 The trends in the coverage for the metal, O and OH-assisted pathway over Pt, Au and Ag step, corner, terrace sites and metal clusters for the formation of (a) glycolic acid and (b) oxalic acid, at 473 K and 1 bar (Error bar = 0.2eV).....	207
Figure 8.1 Rational catalyst design for the removal of organic contaminants from water via catalytic reactions (hydrodechlorination and oxidation reactions)	215
Figure 8.2 Computational modeling for the removal of organic contaminants in waste water over model surfaces, clusters and supported clusters	217
Figure A1. Mechanistic routes for hydrodechlorination of trichloroethylene.....	218
Figure A2. The π -binding modes of trichloroethylene on different Pd facets.....	219

Figure A3. Reactant, transition and product state structures for the first hydrogenation step on the Pd (111), Pd (211), Pd (100) and Pd (110) surfaces. The Pd atoms are displayed in blue, C atoms in grey and H atom in white color (Distances are marked in Å).....	220
Figure A4. Reactant, transition and product state structures for the second hydrogenation step on the Pd (111), Pd (211), Pd (100) and Pd (110) surfaces. The Pd atoms are displayed in blue, C atoms in grey and H atom in white color (Distances are marked in Å).....	221
Figure A5. Reactant, transition and product state structures for the third hydrogenation step (ethylene formation) on Pd (111), Pd (211), Pd (100) and Pd (110) surfaces. The Pd atoms are displayed in blue, C atoms in grey and H atom in white color (Distances are marked in Å)	222
Figure A6. Reactant, transition and product state structures for the hydrogenation of ethylene on the Pd (111), Pd (211), Pd (100) and Pd (110) surfaces. The Pd atoms are displayed in blue, C atoms in grey and H atom in white color (Distances are marked in Å).....	223
Figure A7. Reactant, transition and product state structures for the hydrogenation of ethyl (ethane formation) on Pd (111), Pd (211), Pd (100) and Pd (110) surfaces. The Pd atoms are displayed in blue, C atoms in grey and H atom in white color (Distances are marked in Å)	224
Figure A8. The transition state scaling for the hydrogenation steps on the Pd (111) (■), Pd (211) (●), Pd (100) (▲) and Pd (110) (◆) surfaces	225
Figure A9. The energy diagram for the formation of hydrogen chloride on the Pd (111), Pd (211), Pd (100) and Pd (110) surfaces	226
Figure B1. The diffraction peaks of the Pd/TiO _{2(S)} , Pd/TiO _{2(C)} , TiO _{2(S)} and TiO _{2(C)} catalysts	230
Figure B2. Calibration plot for the varying concentrations of trichloroethylene (TCE)	230
Figure B3. Variation of TCE conversion with time	231
Figure C1. Various binding modes of 4-CP on (1) Pd (111), (2) Pd ₃ Cu (111), (3) Pd ₃ Ag (111) and (4) Pd ₃ Au (111) surfaces	234
Figure C2. The Most Stable Binding Modes of Cl on (1) Pd (111), (2) Pd ₃ Cu (111), (3) Pd ₃ Ag (111) and (4) Pd ₃ Au (111) surfaces.....	235
Figure C3. The Most Stable Binding Modes of H on (1) Pd (111), (2) Pd ₃ Cu (111), (3) Pd ₃ Ag (111) and (4) Pd ₃ Au (111) surfaces.....	235
Figure C4. The Most Stable Binding Modes of HCl on (1) Pd (111), (2) Pd ₃ Cu (111), (3) Pd ₃ Ag (111) and (4) Pd ₃ Au (111) surfaces.....	235
Figure C5. Transition state structures on the Pd (111) surface for the C-Cl bond dissociation step with Cl at the hcp site (I) and Cl at the fcc site (II).....	236

Figure C6. Surface coverage of Cl with varying temperatures and pressures over different surfaces ((1) Pd (111), (2) Pd₃Cu (111), (3) Pd₃Ag (111) and (4) Pd₃Au (111))236

Figure D1. Mechanistic routes for the oxidation of ethylene glycol (EG) via the metal, O and OH-assisted routes to form glycolic acid (GA) and oxalic acid (OA).....237

List of Tables

Table 1.1 Catalytic transformation of organic pollutants	10
Table 2.1 Effect of particle size of the catalyst on the HDC reactions of contaminants	43
Table 2.2 Reactivity of Pd on different supports for the HDC reactions of contaminants.....	48
Table 2.3 Reactivity of different transition metal catalysts on the same support for HDC reactions of contaminants	50
Table 2.4 Comparison of different solvents used for HDC reactions of contaminants.....	60
Table 2.5 Different solvents and hydrogen donors used for HDC reactions of contaminants	63
Table 4.1 Hydrogenation of chlorinated intermediates on different Pd facets	114
Table 4.2 Comparison between ethylene desorption energy and ethylene hydrogenation to ethyl species on different Pd facets.....	125
Table 5.1 The elemental composition, dispersion and metal surface area of the catalysts tested in the HDC reaction of TCE	146
Table 5.2 Conversion of TCE with time at various temperatures.	148
Table 6.1 The calculated lattice constants at which the total energy is minimum for the Pd-based alloys.....	163
Table 6.2 The d-band centers of Pd and Pd-based alloys	170
Table 7.1 Activation energies for the first O-H bond dissociation in EG for the metal-assisted and metal, O and OH-assisted pathway over Ag and Pt metals.....	197
Table 7.2 TOFs of glycolic acid for the metal-assisted and the metal, O and OH-assisted pathways over different transition metals	200
Table B1. Calculated multiplicity for the Pd ₄ clusters	231
Table C1. Formation energies of the species used to construct the MKM.....	232
Table D1. Formation energy of species used in the model. Reference – H ₂ O, CH ₄ and H ₂ .	241